EUKARYOTIC CELL, Apr. 2011, p. 556–564 Vol. 10, No. 4
1535-9778/11/$12.00 doi:10.1128/EC.00244-10

Tracking Glideosome-Associated Protein 50 Reveals the Development and Organization of the Inner Membrane Complex of *Plasmodium falciparum*▽†

Jeffrey A. Yeoman,[1,2] Eric Hanssen,[1,2]‡ Alexander G. Maier,[1,2] Nectarios Klonis,[1,2] Bohumil Maco,[1,2] Jake Baum,[3] Lynne Turnbull,[4] Cynthia B. Whitchurch,[4] Matthew W. A. Dixon,[1,2] and Leann Tilley[1,2]*

La Trobe Institute for Molecular Science[1] and Centre of Excellence for Coherent X-Ray Science,[2] La Trobe University, VIC 3086, Australia; Walter and Eliza Hall Institute of Medical Research, Melbourne 3050, VIC, Australia[3]; and ithree institute, University of Technology Sydney, NSW 2007, Australia[4]

Received 2 October 2010/Accepted 5 January 2011

The most deadly of the human malaria parasites, *Plasmodium falciparum*, has different stages specialized for invasion of hepatocytes, erythrocytes, and the mosquito gut wall. In each case, host cell invasion is powered by an actin-myosin motor complex that is linked to an inner membrane complex (IMC) via a membrane anchor called the glideosome-associated protein 50 (PfGAP50). We generated *P. falciparum* transfectants expressing green fluorescent protein (GFP) chimeras of PfGAP50 (PfGAP50-GFP). Using immunoprecipitation and fluorescence photobleaching, we show that C-terminally tagged PfGAP50-GFP can form a complex with endogenous copies of the linker protein PfGAP45 and the myosin A tail domain-interacting protein (MTIP). Full-length PfGAP50-GFP is located in the endoplasmic reticulum in early-stage parasites and then redistributes to apical caps during the formation of daughter merozoites. In the final stage of schizogony, the PfGAP50-GFP profile extends further around the merozoite surface. Three-dimensional (3D) structured illumination microscopy reveals the early-stage IMC as a doubly punctured flat ellipsoid that separates to form claw-shaped apposed structures. A GFP fusion of PfGAP50 lacking the C-terminal membrane anchor is misdirected to the parasitophorous vacuole. Replacement of the acid phosphatase homology domain of PfGAP50 with GFP appears to allow correct trafficking of the chimera but confers a growth disadvantage.

Despite intense efforts to roll back malaria, it remains one of the most devastating diseases of modern times, with close to 1 million deaths recorded annually (42). *Plasmodium falciparum* is the human malaria species that is responsible for most of the malaria-associated mortality and morbidity. Upon transmission to a human, the parasite undergoes one round of multiplication in the liver prior to initiating the symptomatic asexual blood phase of malaria infection.

The intraerythrocytic cycle commences when a merozoite invades a red blood cell (RBC). The merozoite attaches to ligands on the RBC surface and then reorients so that its apical end can form a tight junction with the RBC membrane (17, 31, 38). Once this junction is established, the parasite uses gliding motility to enter the host cell, forming the parasitophorous vacuole (PV) and PV membrane as it invades (16, 30, 39). The gliding motion is driven by an actin-myosin motor present within the pellicle of the invading merozoite (27).

The pellicle structure is a flattened double-membrane-bound cisterna that subtends the parasite plasma membrane and is known as the inner membrane complex (IMC). Actin filaments, which are thought to lie between the plasma membrane and the IMC (7, 33), are connected via aldolase to an adhesin, which in the asexual blood stages is the merozoite thrombospondin-related adhesive protein (mTRAP). mTRAP is a type I integral membrane protein with a short cytoplasmic tail and an adhesive extracellular domain that may bind to the RBC or to another invasion protein (8). The actin filaments connect to myosin A (myoA) heavy chain (33), which in turn is anchored to the IMC via a light chain or myosin A tail domain-interacting protein (MTIP) (10). Two further IMC proteins, the peripheral protein *P. falciparum* glideosome-associated protein 45 (PfGAP45) and the transmembrane protein PfGAP50, form a complex with myoA and MTIP and together make up what has been called the glideosome, or motor complex (7, 27). Originally described in the related apicomplexan parasite *Toxoplasma gondii* (20), the components of the motor complex have more recently been characterized in *P. falciparum* (9, 22, 26).

The IMC is critical for merozoite motility and viability, but little is known of its origins or of the pathways for trafficking proteins to the organelle. In this work, we use transgenic parasites expressing green fluorescent protein (GFP) fusion constructs of the IMC-resident protein PfGAP50 (PfGAP50-GFP) to study the genesis of the IMC during parasite development. We use live-cell confocal and three-dimensional structured illumination microscopy (3D-SIM) to dissect the amino acid sequence requirements for PfGAP50 trafficking, as well as the timing and order of IMC reorganization during asexual development and merozoite formation.

* Corresponding author. Mailing address: La Trobe University, Biochemistry Department, Plent Rd., Bundoora, VIC 3086, Australia. Phone: (61) 3 9479 1375. Fax: (61) 3 9479 2467. E-mail: L.Tilley@latrobe.edu.au.

‡ Present address: Bio21 Molecular Science and Biotechnology Institute, University of Melbourne, Parkville, VIC 3010, Australia.

† Supplemental material for this article may be found at http://ec.asm.org/.

▽ Published ahead of print on 14 January 2011.

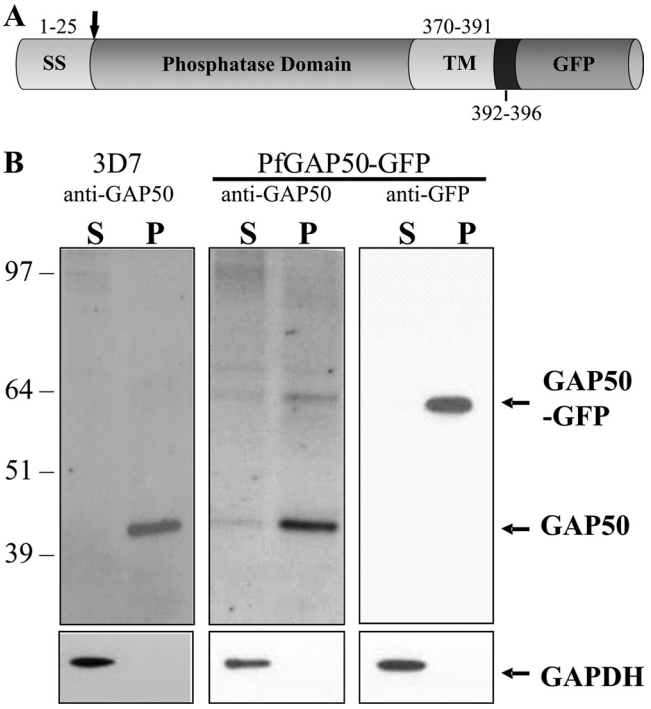

FIG. 1. Schematic diagram of the PfGAP50 chimera construct and Western analysis of PfGAP50-GFP transfectants. (A) The four domains of PfGAP50 are as follows: a predicted signal sequence (SS), an acid phosphatase homology domain, a predicted transmembrane domain (TM), and a short cytoplasmic tail. (B) Late-stage 3D7 parent and full-length PfGAP50-GFP transfectants were enriched, treated with streptolysin O, and then lysed by freeze-thaw cycling. Supernatant (S) and pellet (P) fractions were subjected to Western blotting and probed with antibodies recognizing PfGAP50 or GFP. The blots were reprobed with antibodies recognizing the soluble parasite protein PfGAPDH.

MATERIALS AND METHODS

Parasite culture, transfection, and PfGAP50-GFP constructs. *P. falciparum* parasites (strain 3D7) were maintained in O-type human RBCs from the Melbourne Red Cross Blood Bank in RPMI-HEPES medium supplemented with 5% human serum and 0.5% Albumax (19). Tight synchronization of cultures was achieved using a modification of the method previously described (34). Briefly, schizont stage parasites were purified using 70% (wt/vol) Percoll. Purified parasites were immobilized as a monolayer in a dish coated with concanavalin A. Uninfected RBCs were overlaid for 30 min and then removed to begin a new culture of highly synchronous parasites. The timing of the synchronous culture was measured from the beginning of the 30-min incubation period. Aliquots were taken every hour for confocal microscopic analysis.

PfGAP50 (PlasmoDB gene identifier, PFI0880c) comprises four distinct domains, as shown in Fig. 1A. PfGAP50 is characterized by a hydrophobic N-terminal signal sequence with a predicted cleavage site after amino acid 25, an acid phosphatase homology domain, a transmembrane domain, and a 5-amino-acid predicted cytoplasmic domain (SKNMK). The full-length *PfGAP50* gene was PCR amplified using primers 5′-TCAGAACTCGAGATGAATTATTGTAAA ACCACGTTCC-3′ and 5′-TATGGTACCTTTCATATTTTTTGATAAAAAA GAGGAAGC-3′. A C-terminal $PfGAP50_{1\text{-}369}$ was constructed using the above forward primer and the alternative reverse primer 5′-ACCAATGGTACCTAC AACTCTAACAAAGGTATC-3′. The DNA fragments were digested with XhoI/KpnI (underlined) and cloned into the *P. falciparum* transfection vector pGLUX1 (A. G. Maier, M. T. O'Neill, and A. F. Cowman, unpublished data), which incorporates the human dihydrofolate reductase (hDHFR) cassette for positive selection with the prodrug WR99210 (18). This vector drives transgene expression from the *PfCRT* 5′ promoter region, which has maximal expression in the late ring stages (11). A second mutant, in which the acid phosphatase domain of PfGAP50 is replaced with GFP (PfGAP50ΔAP-GFP), was constructed using overlapping PCR. The PfGAP50 N-terminal and C-terminal domains and the GFP coding sequence were amplified from 3D7 genomic DNA using the following primer pairs. N-terminal, 5′-GATATGTCAATATTTGTATAACACATGA AG-3′ and 5′-TTCTTCTCCTTTACTCCAATCACCCAAAGA-3′; C-terminal, 5′-GATGAACTATACAAATTTGTTAGAGTTGTA-3′ and 5′-TAACATTTA TTCATTATAATATTTATCATATTATATATATA-3′; and GFP, 5′-AGTAAA GGAGAAGAACTTTTCACTGGAGTTGTC-3′ and 5′-TTTGTATAGTTCAT CCATGCCATGTGTAATCCC-3′. The final construct was generated by PCR using the overlapping product as a template and 5′-TCAGAACTCGAGATGA ATTATTGTAAAACCACGTTCC-3′ and 5′-GCGCTTAATTAATTATTTCA TATTTTTTGATAAAA-3′. The PCR product was digested with XhoI/PacI (underlined), purified, and cloned into the pGLUX1 vector. 3D7 parasites were transfected with 100 μg of purified plasmid DNA as previously described (13). The episomal constructs were maintained by culturing them in the presence of 10 nM WR99210.

Western analysis of PfGAP50-GFP transgenic parasites. Highly synchronized late-stage PfGAP50-GFP parasites were purified using 70% (wt/vol) Percoll and treated with streptolysin O (SLO) (1.5 U/μl final concentration) at 37°C for 15 min to remove hemoglobin (40). The cells were lysed with 3 rapid freeze-thaw cycles in phosphate-buffered saline (PBS), and the soluble and insoluble fractions were separated by centrifugation at 12,000 × *g* for 10 min at 4°C. Proteins were separated on 4 to 12% SDS NuPage gels (Invitrogen) under reducing conditions and transferred onto nitrocellulose membranes. The membranes were probed with either mouse anti-GFP (Roche; 1:500), anti-PfGAP45 (1/500 dilution), anti-PfGAP50 (1:500) (9) or anti-MTIP (22), or rabbit anti-PfGAPDH (36), followed by horseradish peroxidase-conjugated sheep anti-mouse or anti-rabbit secondary antibodies (Promega; 1:5,000). Western blots were developed using enhanced chemiluminescence.

Immunoprecipitation of IMC components. Highly synchronized late-stage parasites were purified over 70% (wt/vol) Percoll, and proteins were extracted by incubating them on ice for 15 min in RIPA buffer (1% octylphenoxypolyethoxyethanol [IGEPAL CA-630], 150 mM NaCl, 0.5% sodium deoxycholate [DOC], 0.1% sodium dodecyl sulfate [SDS], 50 mM Tris, pH 7.4). Soluble and insoluble fractions were separated by centrifugation at 12,000 × *g* for 10 min at 4°C. Soluble lysates were incubated for 1 h at 4°C using the rabbit antibodies anti-PfGAP45, anti-GFP, and anti-MTIP and preimmune serum. A 1:1 ratio of protein-A/G–Sepharose was used for immunoprecipitation (IP). IP lysates were separated by SDS-PAGE and analyzed by Western blotting using mouse antibodies against GFP, PfGAP45, or PfMTIP. Western blots were developed as described above.

Light microscopy and immunofluorescence. For immunofluorescence, air-dried thin smears were fixed for 10 min at room temperature in 100% acetone, and antibody labeling was performed as explained below. Alternatively, aliquots of culture were washed in PBS and fixed for 20 min at room temperature in 2% paraformaldehyde, 0.008% glutaraldehyde. The cells were permeabilized with 0.1% Triton X-100 for 5 min at room temperature prior to antibody incubation. The prepared cells were incubated for 1 h with the following antibodies diluted in 3% bovine serum albumin (BSA) in PBS: mouse anti-GFP (1:500; Roche), rabbit anti-PfGAP45 (1:500), rabbit anti-PfGAP50 (1:500), rabbit anti-RhopH3 (41) (1:500), and rabbit anti-Bet3 (2) (1:500), followed by Alexa Fluor 488 or 568 anti-IgG (Molecular Probes). Cells were washed in PBS, resuspended in Dako mounting medium, and viewed using a Leica TCS-SP2 confocal fluorescence microscope. For labeling of the endoplasmic reticulum (ER) cultures, ER-Tracker Blue-White DPX (0.25 μM; Invitrogen Corporation) was added to an aliquot of a culture for 30 min at 37°C. The cells were resuspended in fresh complete medium, and the ER fluorescence pattern was examined using an Olympus IX81 fluorescence microscope with a DAPI (4′,6-diamidino-2-phenylindole) filter set.

For live-cell confocal imaging of transfectants, 3 μl of culture (3% hematocrit; 5 to 10% parasitemia) was sealed under a coverslip and viewed on a Leica TCS-SP2 or a Zeiss LSM 510/FCS confocal microscope within 20 min of mounting. Fluorescence recovery after photobleaching (FRAP) was performed on a Zeiss LSM 510/FCS, as previously described (28). Selected regions were photobleached using a 488-nm laser at 80% intensity for 0.1 s. Fluorescence images were acquired before, immediately after, and 3 min after bleaching.

3D-SIM (37) was implemented on a DeltaVision OMX 3D-SIM (*o*ptical *m*icroscope, experimental) at the Microbial Imaging Facility of the University of Technology Sydney. The samples were excited using 405-nm and 488-nm lasers and imaged using emission filters of 419 to 465 nm and 500 to 550 nm, with a 100× 1.4-numerical aperture (NA) oil lens and multichannel simultaneous-imaging capability (electron-multiplying charge-coupled device cameras; >90% quantum efficiency; 512 by 512 pixels). Aliquots of culture were adjusted to a final concentration of 2% paraformaldehyde, 0.008% glutaraldehyde and resus-

pended in 50% Vectashield antifade mounting medium (Vectorlabs), containing DAPI, in PBS. All images were processed using NIH Image J version 1.42 (http://rsbweb.nih.gov/ij/).

Electron microscopy. Transmission electron microscopy (EM) and tomography were performed as previously described (14, 23). Briefly, tightly synchronized early- or late-schizont-stage 3D7 parasites were fixed, embedded, and stained. Seventy-nanometer-thick sections were observed at 120 keV using a JEOL-2010HC (Japan) transmission electron microscope (La Trobe University, EM Unit). For electron tomography, 200- or 300-nm sections were cut, stained, and observed at 200 keV on a Tecnai G^2 F30 (FEI Company) transmission electron microscope (Bio21 Institute, Melbourne, Australia). Tilt series were collected and reconstructed to generate cell models as described previously (1).

RESULTS

Full-length PfGAP50-GFP is expressed in transfected *P. falciparum*. To examine the genesis and origin of the IMC, *P. falciparum* transfectants expressing full-length PfGAP50 tagged at the C terminus with GFP were generated (Fig. 1A). Mature-stage parasite cultures of the parent (3D7) and transfected (PfGAP50-GFP) lines were harvested and selectively lysed with streptolysin O to remove the host cell hemoglobin. The isolated parasites were disrupted by freeze/thawing, and the supernatant and pellet fractions were subjected to Western blotting. Anti-PfGAP50 recognizes a band of 42 kDa in the pellet fraction of 3D7-infected RBCs (Fig. 1B, left), as reported previously (9), and an additional band of 64 kDa in the PfGAP50-GFP transfectant (Fig. 1B, middle). The relative intensity of the upper band indicates that PfGAP50-GFP is expressed at a lower level than endogenous PfGAP50. When the blotted lysates of the PfGAP50-GFP transfectants were probed with anti-GFP, only the 64-kDa protein species was detected (Fig. 1B, right), with no reactivity in 3D7 parasites or uninfected RBCs (data not shown). The apparent molecular masses of PfGAP50 and PfGAP50-GFP are in rough agreement with the predicted masses after cleavage of the signal sequence (41.5 kDa and 68.3 kDa, respectively). The presence of PfGAP50 and PfGAP50-GFP in the pellet fraction indicates that they are membrane associated. The blots were stripped and reprobed with anti-PfGAPDH to compare loading levels and to validate the lysis procedure (Fig. 1B, bottom).

Full-length PfGAP50-GFP is incorporated into the glideosome complex. Endogenous PfGAP50 and PfGAP45 form part of the glideosome complex that is associated with the IMC (9). To determine whether full-length PfGAP50-GFP participates in this complex, we immunoprecipitated IMC components from the transfectants. Mature-stage parasite-infected RBCs were enriched and solubilized using a detergent-containing buffer. Cleared soluble lysates were immunoprecipitated with a range of antibodies (Fig. 2). When a Western blot of the precipitated samples was probed with mouse anti-GFP antibodies, a band corresponding to full-length PfGAP50-GFP (64 kDa) was detected in samples precipitated with anti-PfGAP45, anti-MTIP, and anti-GFP sera, but not with the preimmune serum (Fig. 2). The lysate sample precipitated using anti-GFP contained both PfGAP45 and PfMTIP (Fig. 2, right lanes). Mouse anti-PfGAP45 antiserum detected a doublet at 37 or 39 kDa, while anti-PfMTIP recognized a 27-kDa band. This demonstrates that full-length PfGAP50-GFP is in complex with endogenous PfGAP45 and PfMTIP.

Live-cell imaging reveals marked rearrangements of the IMC during parasite development. To follow the movement

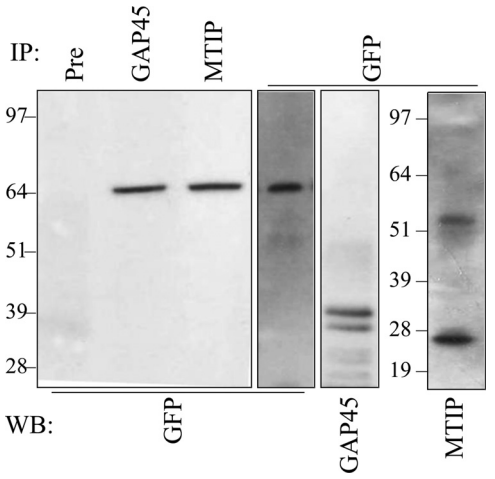

FIG. 2. PfGAP50-GFP interacts with PfGAP45 and PfMTIP. Proteins were detergent solubilized from enriched, mature-stage PfGAP50-GFP transfectants. The extract was immunoprecipitated (IP) using rabbit preimmune serum (Pre), anti-PfGAP45, anti-PfMTIP, or anti-GFP. Western blots (WB) of the pellet fractions were probed with mouse anti-GFP, anti-PfGAP45, or anti-PfMTIP. The antibodies used for IP are shown at the top of the blot, and those for WB are shown at the bottom.

and redistribution of PfGAP50 during *P. falciparum* development, we synchronized a parasite culture to within a 2-h window (34). Confocal microscopy analysis of cells reveals a marked reorganization of the PfGAP50-GFP as the parasite matures (Fig. 3; see Fig. S1 in the supplemental material). In ring and early- to mid-trophozoite stage parasites, PfGAP50-GFP is present within the parasite in a pattern that is reminiscent of that in the ER (Fig. 3; see Fig. S1, top, in the supplemental material). In the late-trophozoite/early-schizont stage, the fluorescence pattern becomes more looped (Fig. 3, 38 to 40 h). At 40 to 42 h postinfection, the PfGAP50-GFP starts to accumulate into foci, which by 44 h have developed into distinct puncta at the periphery of the parasite (Fig. 3). The punctate fluorescent structures are close to bright dots in the differential interference contrast (DIC) image that probably represent the rhoptry organelles (see Fig. S1, schizonts, in the supplemental material). In the final stage of schizogony (~46 h postinvasion), the fluorescence appears to redistribute around the periphery of the daughter merozoites (Fig. 3; see Fig. S1 in the supplemental material).

Full-length PfGAP50-GFP is trafficked via the ER to apical regions of developing merozoites. In an effort to determine the nature of the subcellular compartments with which PfGAP50-GFP is associated, we undertook colabeling with different markers. In the early stages of development, ER-Tracker labels a reticular structure that largely overlaps with the PfGAP50-GFP location (Fig. 4A, top). The profile is dispersed and coincident with the pattern for the ER-resident protein PfERC (ER calcium binding protein) in trophozoite stage parasites (Fig. 4B, top).

This is perhaps surprising, given that PfGAP50 has previously been reported to be a component of the IMC, which lies under the merozoite plasma membrane. To ensure that this was not an artifact due to expression of PfGAP50-GFP under a heterologous promoter, we examined samples of the 3D7

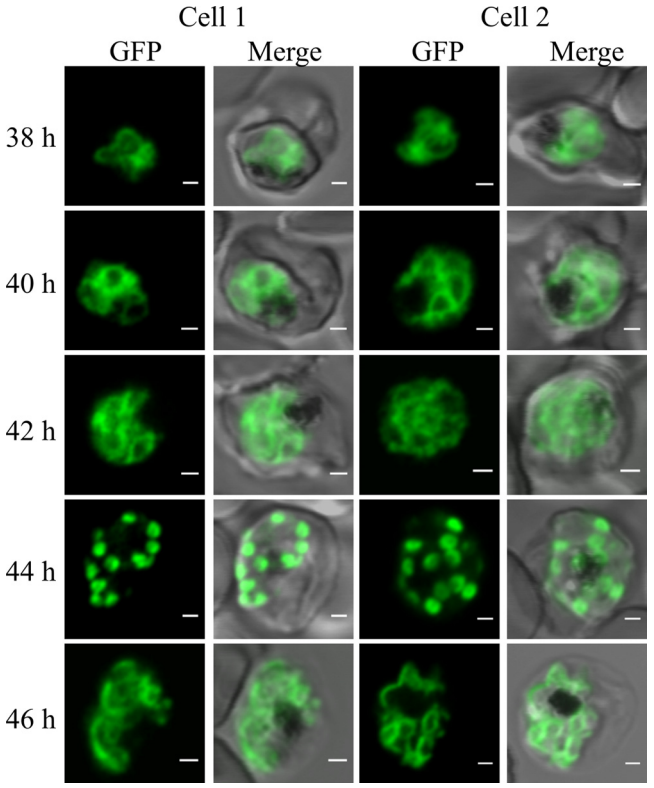

FIG. 3. Dynamics of PfGAP50-GFP-labeled compartments in live transfectants. Shown is live confocal fluorescence microscopy of highly synchronized PfGAP50-GFP transfectants. Single section scans (collected at 25 μs/pixel) from different cells at 2-h intervals in the schizont stage are shown (2 cells are represented per time point). At 40 to 42 h after invasion, reticular structures with looped extensions and focal concentrations of PfGAP50-GFP are apparent, coalescing into punctate structures by 44 h. The PfGAP50-GFP-containing structures then appear to expand around each of the daughter merozoites. A more extended time series is shown in Fig. S1 in the supplemental material. Bars = 1 μm.

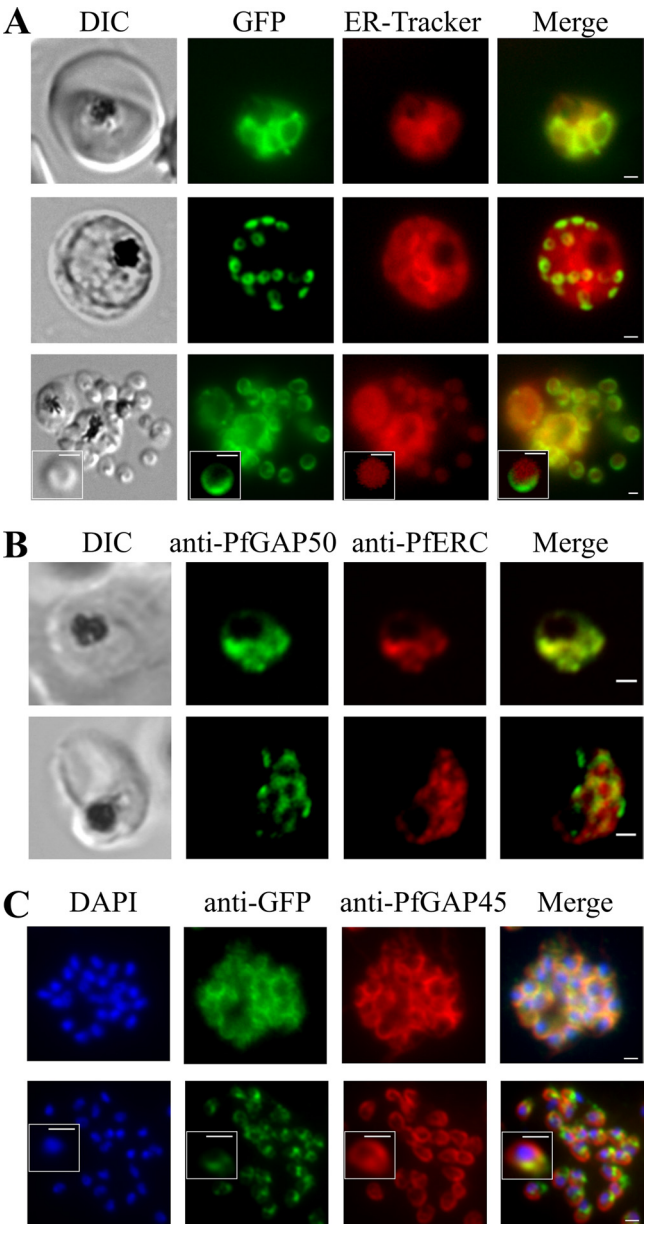

FIG. 4. PfGAP50 is located in the ER prior to recruitment to the IMC. (A) Parasites expressing PfGAP50-GFP (green) were incubated with ER-Tracker (depicted in red). The GFP and ER-Tracker fluorescence signals are colocated in trophozoite stage parasites. Upon relocation of GFP fluorescence to the apical ends of nascent merozoites during the early schizont stage, the reticular ER-Tracker labeling persists. PfGAP50-GFP is concentrated at one pole of released merozoites, while ER-Tracker labels internal structures. (B) Fixed-cell immunofluorescence microscopy of the 3D7 parent strain labeled with antibodies raised against PfGAP50 (green) and PfERC (red). (C) Immunofluorescence microscopy of PfGAP50-GFP transfectants at the mature- and ruptured-schizont stages labeled with anti-GFP (green), anti-PfGAP45 (red), and DAPI (blue). Bars = 1 μm.

parental strain. An antiserum raised against endogenous PfGAP50 (9) gives a labeling pattern that shows almost complete overlap with that observed for PfGAP50-GFP in both trophozoite and schizont stage parasites (see Fig. S2A in the supplemental material). As described above, in schizont stage parasites, the GFP chimera redistributes to punctate structures located around the periphery of the dividing parasite (Fig. 4A, middle). At this stage, ER-Tracker labels reticular structures, presumably the ER, within the parasite with a diffuse staining pattern quite unlike that of PfGAP50-GFP. Similarly, in immunofluorescence images of schizont stage 3D7 parasites, PfGAP50 and PfERC are not colocated (Fig. 4B, bottom). The PfGAP50-containing structures are not Golgi apparatus, as the labeling patterns for PfGAP50-GFP and the Golgi marker, PfBet3 (2), are quite distinct (see Fig. S2B in the supplemental material).

In rupturing schizonts, PfGAP50-GFP is located at the periphery of individual daughter cells and appears to extend from one pole, while ER-Tracker labels the inside of individual merozoites (Fig. 4A, bottom). These data indicate that PfGAP50-GFP is redistributed from the ER to separate structures within the dividing cell. Colabeling with the rhoptry marker RhopH3 (41) confirms the location of PfGAP50-GFP, extending from the apical region of the daughter merozoites (see Fig. S2C in the supplemental material).

We compared the location of PfGAP50-GFP in the late

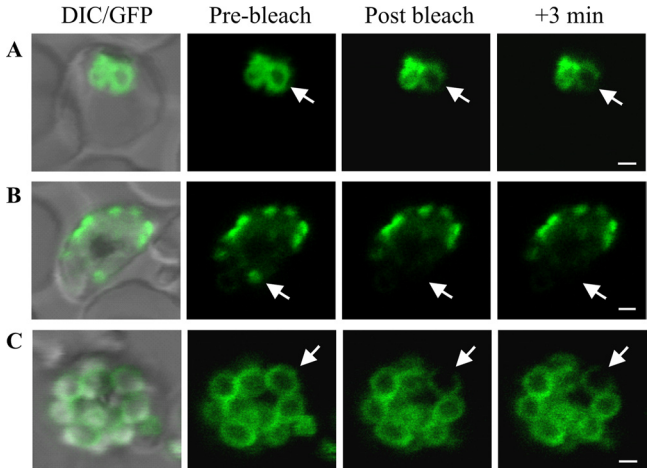

FIG. 5. Photobleach analysis of PfGAP50-GFP organization. The panels are prebleach images with and without DIC overlay and postbleach images after application of a laser pulse at the positions indicated by arrows. (A) A region of the ER in an early-trophozoite stage parasite shows complete loss of fluorescence at the point of bleaching, partial loss from a connected compartment, and little loss from an adjacent compartment. There was no recovery after 3 min. (B) Application of a laser pulse to PfGAP50-GFP in an apical cap in an early schizont ablates fluorescence with no recovery from adjacent structures. (C) Spot bleaching of a region of PfGAP50-GFP in a region of a mature merozoite results in complete loss of fluorescence at the point of bleaching, with little loss from other regions of the same merozoite or from adjacent merozoites. Bars = 1 μm.

schizont stage with that of the known IMC-resident protein PfGAP45 (Fig. 4C, top). In schizont stage parasites, these proteins appear to be largely colocated in a region of each daughter merozoite away from the nucleus (i.e., at the apical end). This is consistent with coparticipation in the IMC. Interestingly, in released merozoites, the locations of PfGAP45 and PfGAP50-GFP are not completely overlapping (Fig. 4C, bottom), suggesting that PfGAP50-GFP is reorganized after merozoite release.

In an effort to determine the physical organization of PfGAP50 within the IMC, we performed FRAP studies of PfGAP50-GFP-labeled structures at different stages of parasite development. In the trophozoite stage, application of an intense laser pulse caused selective bleaching of PfGAP50-GFP in a region of the ER (Fig. 5A). There was partial loss of fluorescence from adjacent regions during the bleach pulse and no recovery of the signal from other regions of the ER over a period of 3 min. This indicates that at least part of the PfGAP50-GFP is present in a state that shows restricted diffusion. When the PfGAP50-GFP had redistributed to the apical caps, there was no recovery of the signal after photobleaching, indicating that PfGAP50-GFP from other caps cannot diffuse into this compartment (Fig. 5B). When the PfGAP50-GFP has redistributed around the periphery of the daughter merozoites (Fig. 5C), loss of signal is restricted to the bleach point and does not recover. This indicates that PfGAP50-GFP is present in a protein complex that restricts lateral diffusion within the membrane.

PfGAP50 is located in an apical IMC cap in developing merozoites. The punctate PfGAP50-GFP-labeled structures observed in developing merozoites are intriguing; however, their small size limits the information that can be obtained using conventional optical microscopy. 3D-SIM has recently been developed as a method for imaging fluorescently labeled samples with improved resolution (37). We used 3D-SIM to image PfGAP50-GFP in parasites that are colabeled with DAPI (Fig. 6).

The characteristic PfGAP50-GFP-labeled punctate structures are apparent in a parasite with 8 nuclei (Fig. 6A and C). At higher resolution, it is evident that the PfGAP50-GFP-containing caps are located at the apical ends of nascent merozoites and form flat, ellipsoid structures, each with two unlabeled "pores." The average dimensions of these pores were estimated to be 110 ± 40 nm by 140 ± 40 nm (n = 18). The nature of these structures and their organization relative to the parasite nuclei can be best appreciated in a rotation of the 3D-SIM reconstruction presented in movie S1 in the supplemental material.

As the eight nuclei start to divide, the PfGAP50-GFP-labeled structures appear to be pulled apart, with the pores opening to give a claw-like appearance (Fig. 6B and D). These structures are organized in pairs, with the cavities facing each other (Fig. 6D, arrow; for a rotation of the 3D-SIM reconstruction, see movie S2 in the supplemental material). The average length of the cavity is 230 ± 40 nm, while the width in its central region is 130 ± 30 nm (n = 18). These may represent the apical caps of separating daughter cells in which the nascent IMC structures are pulled apart.

We performed EM on schizont stage parasites in an effort to find an ultrastructural correlate of these doubly punctured ellipsoids. In early-schizont stage parasites, apical prominences are observed on the developing merozoites at either side of a single nucleus (Fig. 6G and H). The apical prominence is formed close to a mitotic spindle (Fig. 6H, m). The multiple membranes and cytoskeletal components (microtubules) of the nascent pellicle give this region an electron-dense appearance (Fig. 6G and H, arrowheads). Later in development, separate structures can be observed at the apical ends of the dividing merozoites (Fig. 6I and J, arrowheads), which likely correspond to the separating claw-like structures seen by 3D-SIM. The "pores" in the PfGAP50-GFP-labeled cap presumably correspond to the central region of the cytoskeletal annulus at the apex of the cell. An electron tomogram was generated from a section through a mature merozoite, and the tubulin rings are observed in cross-section in a virtual section from the tomogram (Fig. 6K, arrows). Four serial electron tomograms collected through mature merozoites were rendered to generate a model of a mature merozoite (Fig. 6L), with the apical rings depicted in blue. These polar rings provide a structure through which the rhoptry necks (indicated in burnt orange) are connected to the parasite surface. The inner, middle, and outer polar rings have diameters of approximately 120 nm, 180 nm, and 240 nm. We interpret the 3D-SIM data to suggest that PfGAP50 is recruited to the developing IMC and that the IMC forms a membrane collar surrounding the apical pore.

As the schizont develops further, the PfGAP50-GFP appears to extend around the surface of the parasite (Fig. 6E and F). The apical pores remain visible, but due to the extension of the IMC around the periphery of the merozoite, which dilutes the PfGAP50-GFP, they are less prominent. The change in IMC organization is best appreciated by comparing the divid-

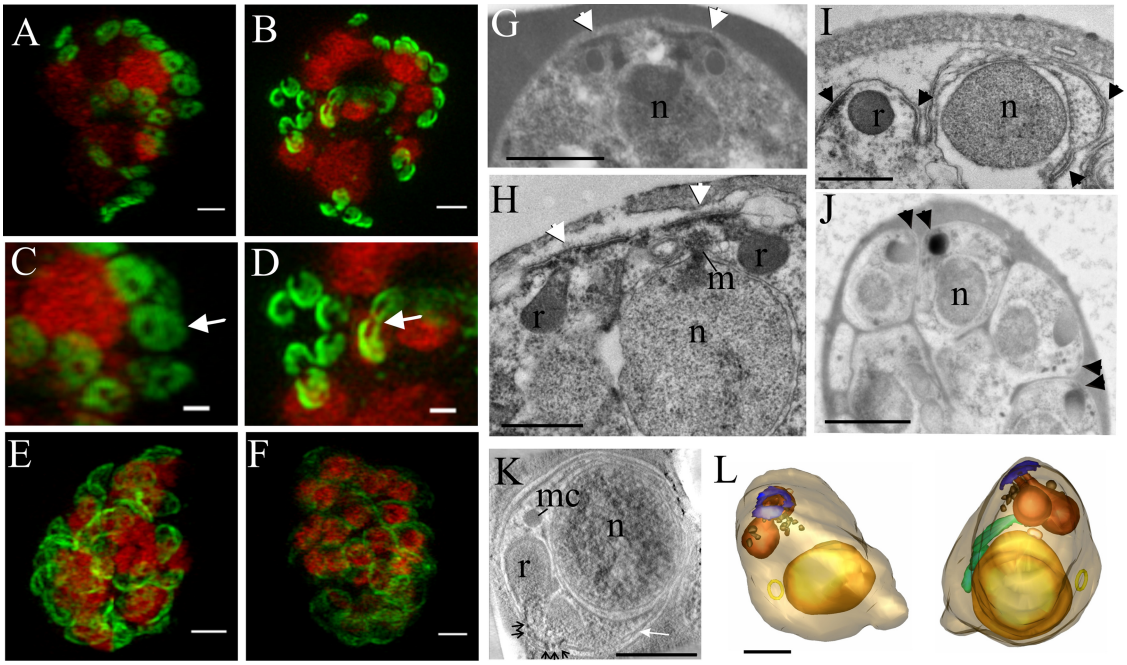

FIG. 6. The IMC forms around the apical pore of developing merozoites. 3D-SIM was performed on parasites expressing PfGAP50-GFP (green) labeled with DAPI nuclear stain (depicted in red). (A and C) Schizont with eight nuclei, each with two associated PfGAP50-GFP-containing ellipsoids. Each ellipsoid has two unlabeled "pores" (arrow). (B and D) A schizont with eight nuclei that are undergoing division showing the PfGAP50-GFP-containing structures separating into claw-like structures (arrow). (E and F) Mature schizonts in which the PfGAP50-GFP fluorescence is more evenly distributed around the periphery of the parasite. (G and H) Transmission EM (TEM) images of early schizonts with electron-dense apical prominences with overlying membrane caps (arrowheads) forming in pairs on either side of a nucleus (n). The apical caps are connected to the underlying electron-dense rhoptries (r) and form close to a mitotic spindle (m). (I) TEM image of a maturing schizont showing invagination of the parasite plasma membrane around the daughter cells and separation of the apical caps (arrowheads). (J) TEM image of a mature schizont showing electron-dense structures at the apical ends of closely apposed daughter cells (arrowheads). (K) Selected virtual section (22 nm) through a tomogram showing a merozoite developing within a schizont. The electron-dense polar rings are indicated with black arrows, and the IMC with a white arrow. A microneme (mc) is visible. (L) Rendered tomographic reconstructions of merozoites, generated from serial sections through the schizont shown in panel K, showing the nucleus in yellow, rhoptries in burnt orange, dense granules in brown, the polar rings in blue, the mitochondrion in green, and a cytostomal ring as a yellow circle. Rotations of the 3D projection in panels A, B, E, and F are presented in movies S1 to S4 in the supplemental material. Bars = 1 μm (A to F, G, and J) and 500 nm (H, I, K, and L).

ing schizonts in movies S1 and S2 in the supplemental material with the more mature schizonts in movies S3 and S4.

The C-terminal transmembrane domain of PfGAP50 is needed for correct trafficking to the IMC. In *T. gondii*, the transmembrane domain and the short C-terminal segment of PfGAP50 are needed for correct assembly into the glideosome complex (20). In an effort to determine whether the same region of PfGAP50 is needed for correct trafficking and assembly in *P. falciparum*, we generated transfectants expressing GFP chimeras of two different PfGAP50 mutants (Fig. 7A) and examined their intracellular locations.

Live-cell fluorescence microscopy of the PfGAP50$_{1\text{-}369}$-GFP transfectants (lacking the C-terminal hydrophobic and cytoplasmic domains) (Fig. 7B) indicates that the chimera is in the PV, with some protein being transferred to the digestive vacuole (Fig. 7B, middle). Colabeling of these cells with ER-Tracker (Fig. 7B, bottom) confirms that the PfGAP50$_{1\text{-}369}$-GFP fluorescence is outside the region of the ER. The data suggest that the N-terminal signal peptide directs entry into the secretory pathway and that, in the absence of amino acids 370 to 396, it follows the default trafficking pathway to the PV (3). This confirms that the C-terminal transmembrane and cytoplasmic domains are required for correct trafficking of PfGAP50 to the IMC in *P. falciparum*.

Mature stage PfGAP50$_{1\text{-}369}$-GFP transfectants were released with streptolysin O and then ruptured, and the pellet and supernatant fractions were subjected to Western analysis. The transfectants express a protein of 61 kDa (Fig. 7C), which is similar to the anticipated size of PfGAP50$_{1\text{-}369}$-GFP after cleavage of the signal sequence, as well as a protein of 26 kDa, which likely represents the protease-resistant core of GFP. The full-length chimera is largely released into the supernatant fraction, suggesting that it is a soluble protein. The cytoplasmic protein PfGAPDH shows a similar solubility profile (Fig. 7C, bottom).

The acid phosphatase homology domain of PfGAP50 is not needed for correct trafficking to the IMC. PfGAP50 has a central domain that exhibits ~25% identity to different purple acid phosphatases of plants and animals. To determine whether this domain is needed for trafficking to the IMC, we generated *P. falciparum* transfectants episomally expressing a construct in which the acid phosphatase homology domain is replaced by GFP (Fig. 7A). Live-cell fluorescence microscopy reveals that the PfGAP50ΔAP-GFP chimera has a fluores-

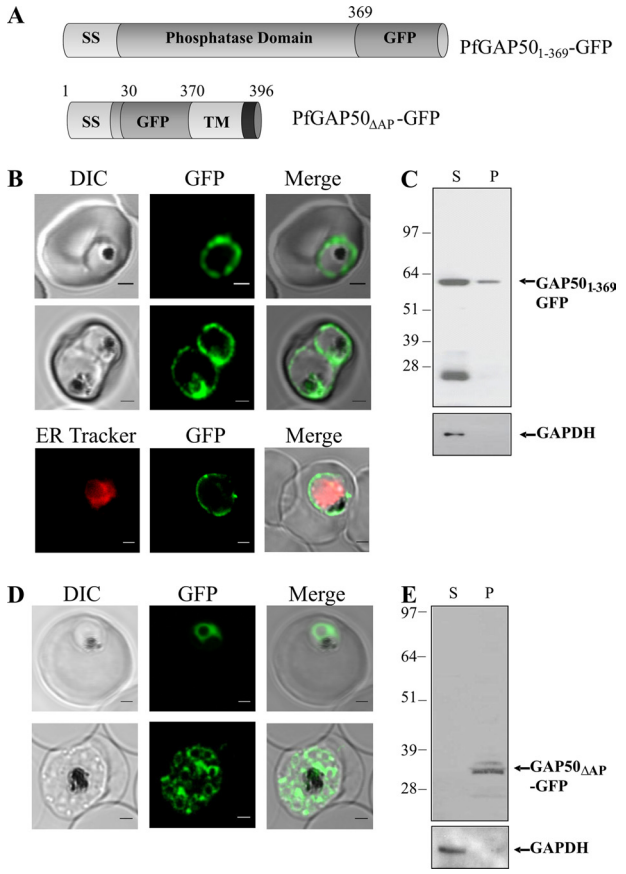

FIG. 7. The C terminus of PfGAP50 is required for correct trafficking. (A) A truncation mutant of PfGAP50 lacking the C-terminal domains (PfGAP50$_{1-369}$-GFP) and a mutant in which the acid phosphatase homology domain is replaced with GFP (PfGAP50$_{\Delta AP}$-GFP) were generated. (B and C) Location and solubility of episomally expressed PfGAP50$_{1-369}$-GFP. (B) Live confocal fluorescence images of trophozoite and schizont stage parasites (top 2 panels) show mistrafficking of PfGAP50$_{1-369}$-GFP to the PV outside the region labeled with ER-Tracker (bottom). Bar = 1 μm. (C) Enriched PfGAP50$_{1-369}$-GFP transfectants were treated with streptolysin O, followed by freeze-thaw cycling. Supernatant (S) and pellet (P) fractions were subjected to Western blotting, probed with antibodies recognizing GFP, and then reprobed with anti-PfGAPDH. (D and E) Location and solubility of episomally expressed PfGAP50$_{\Delta AP}$-GFP. (D) Live-cell images show a fluorescence pattern similar to that of the full-length PfGAP50-GFP. Bar = 1 μm. (E) Late-stage parasites expressing PfGAP50$_{\Delta AP}$-GFP were harvested and lysed, and the Western blot of the pellet and supernatant fractions was probed with mouse anti-GFP.

cence pattern similar to that of full-length PfGAP50-GFP (Fig. 7D). This suggests that the phosphatase domain is not required for correct trafficking of PfGAP50 to the IMC. Western analysis reveals a protein with an apparent molecular mass of 34 kDa (as expected) that is present in the pellet fraction (Fig. 7E), as for full-length PfGAP50-GFP. Unfortunately, these domain-swapped transfectants grew poorly and were lost within 2 to 3 weeks of the first appearance of fluorescent parasites, and we were unable to obtain sufficient material to confirm an interaction with other IMC proteins by immunoprecipitation analyses. The data suggest that, while not essential for trafficking to the IMC, the acid phosphatase domain may play an important role in PfGAP50 function.

DISCUSSION

The IMC of the merozoite is a cisternal structure that is flattened against the plasma membrane of the developing merozoite. It plays a critical role in anchoring the actin-myosin motor that drives invasion. The IMC-associated glideosome complex has been well studied in *T. gondii* and more recently in *Plasmodium*; however, some aspects of its genesis and assembly remain poorly understood.

We generated transfectants expressing an IMC protein, PfGAP50, fused to GFP. We showed that in schizont stage parasites, the chimera is membrane associated, is colocated with the endogenous IMC-resident proteins PfGAP45 and PfGAP50, and coprecipitates with PfGAP45 and MTIP. This demonstrates that PfGAP50-GFP is correctly trafficked to the IMC and is able to participate in a complex with endogenous IMC proteins. The data are consistent with a previous report for *T. gondii* GAP50-yellow fluorescent protein (YFP), which is correctly targeted to the IMC of nascent daughter parasites (20). An antiserum to *T. gondii* GAP45 (TgGAP45) was shown to immunoprecipitate TgMyoA, TgGAP50, TgGAP45, and TgMLC1, along with the TgGAP50-YFP fusion protein (20). The fact that the C-terminal GFP fusion does not interfere with the binding of PfGAP50 to PfGAP45 is at first surprising. It is possible that the binding interface involves more than the 5 amino acids of the cytoplasmic domain of PfGAP50 or that additional proteins are required for complex stability. Indeed, it has been reported that PfGAP45 is both myristoylated and palmitoylated (35). This may facilitate penetration of PfGAP45 into the bilayer, providing a larger interaction area.

While the IMC and many of its components have been well studied, little is known of its origin, its assembly at the apical end of the daughter merozoite, or its redistribution during merozoite development. It seems possible that PfGAP50 might play a role in initiation of the IMC, given that *PfGAP50* transcription is initiated during the ring stage, peaking in the mid-trophozoite stage (29). In contrast, other IMC components, such as PfGAP45 and MyoA, are transcribed only in late trophozoites.

Using tightly synchronized parasites and live-cell imaging, we found that PfGAP50-GFP is associated with the ER of late-ring to mid-trophozoite stage parasites. The GFP-tagged PfGAP50 construct used in this study is expressed using the PfCRT promoter rather than the endogenous PfGAP50 promoter, and there may be some differences in the timing of expression of the tagged and untagged proteins. However, we confirmed that endogenous PfGAP50 is also colocated with the ER-resident protein PfERC at this stage of development. As the parasite matures, the PfGAP50-GFP-labeled structures appear to loop out and then coalesce as punctate structures at the parasite periphery. The data strongly suggest that the IMC originates from the ER, although the mechanism by which this occurs remains unclear. It is possible that initiation of the expression of binding partners is the trigger that causes redistribution of PfGAP50 to the IMC. Our data are supported by data from *T. gondii* suggesting that the IMC is derived from the ER (15), although in *T. gondii*, the organization is somewhat different, as both the mother and daughter cells have an IMC. Another study suggested that the IMC is derived from the Golgi apparatus (25). While we cannot rule out participation

of Golgi components in the generation of the IMC, PfGAP50 does not accumulate in that compartment.

By the time the schizont has developed to the 8-nucleus stage (~44 h postinvasion), PfGAP50-GFP is present in doughnut-shaped puncta at the periphery of the parasite. Doughnut-shaped IMC compartments have been observed previously for parasites labeled with reagents recognizing PfGAP45 (12, 24) or the novel IMC proteins PfGAPM1 (12) and MAL13P1.130 (24). The punctate PfGAP50-GFP-labeled structure that forms at the apical end of each developing merozoite is intriguing, but its small size limits the information that can be obtained using conventional light microscopy, which is restricted to resolving features with dimensions about half the wavelength of the illuminating photons. Recently, techniques have been developed that circumvent the diffraction limit of light (37). We used 3D-SIM to obtain more detailed information about the architecture of the nascent IMC in PfGAP50-GFP transfectants. We found that the IMC precursor is present as a flattened ellipsoid that is punctured by two holes; this structure separates into two apposing claw-shaped structures as the nucleus starts to divide.

Ultrastructural studies of early-schizont stage parasites reveal an electron-dense protrusion at the apical end of each developing merozoite. This apical prominence is the site of the assembly of three tubulin-based annuli called the polar rings that lie underneath the plasma membrane in this region of the cell (4–6). In early-stage schizonts, the IMC membrane is observed as a membrane cap in the region of the cytoskeletal rings. It is possible that an interaction of PfGAP50 (or associated proteins) with the newly formed polar rings may initiate the relocation of PfGAP50 from the ER to the apical prominence. Our data are consistent with a previous EM study showing that the merozoite IMC is formed close to endomitotic spindles (5).

A previous ultrastructural study reported that the IMC cisterna extends radially from the apical rings, leaving a central region that is free of cisternal membrane (5). Thus, the holes in the PfGAP50-GFP-labeled nascent IMC presumably represent the region occupied by the polar rings (4, 6). As the daughter merozoites form in the final stages of schizogony, the PfGAP50-GFP profile extends further around the surface of the nascent daughter cells; this is consistent with EM data showing the extension of the IMC around the developing merozoites. A model of the proposed reorganization of PfGAP50 during IMC development is illustrated in Fig. S3 in the supplemental material.

PfGAP50 and the related TgGAP50 exhibit 20 to 25% identity to purple acid phosphatases of various plants and animals (20). As some of the amino acids that are considered critical for enzyme activity are mutated in TgGAP50, it has been assumed that apicomplexan GAP50 is an inactive homologue of the acid phosphatase family (20). However, recently, a recombinantly expressed version of the acid phosphatase homology domain of PfGAP50 has been generated and shown to have activity as a small-molecule phosphomonoester hydrolase (32). The recombinant enzyme exhibited a broad substrate profile with optimal activity at pH 5 to 7.

Müller et al. (32) studied the intracellular location of PfGAP50. In contrast to our work, these authors concluded that PfGAP50 is trafficked to the parasite plasma membrane and subsequently engulfed in the digestive vacuole. Their study involved the generation of transfectants expressing a chimera comprising the first 99 amino acids of PfGAP50 linked to GFP. This chimera enters the secretory pathway and is trafficked to the PV and, in part, to the digestive vacuole. This is similar to the pattern we observed for the PfGAP50 mutant lacking the C-terminal hydrophobic domain. Similarly a YFP chimera of TgGAP50 lacking the C-terminal 6 amino acids was not incorporated into the glideosome complex (20). We suggest that trafficking of PfGAP50 to the PV and digestive vacuole occurs only in the absence of the C-terminal membrane anchor, which we have shown is essential for correct trafficking and membrane association of PfGAP50. Müller et al. (32) also generated transfectants expressing GFP linked to full-length PfGAP50 and reported that the fluorescence was present in the ER in trophozoite stage parasites. This is in agreement with our data; however, they did not investigate the location of the full-length chimera in schizont stage parasites. Our data suggest that correctly trafficked full-length protein is initially resident in the ER and then relocates to the inner membrane complex of nascent daughter merozoites.

Müller et al. (32) suggested that PfGAP50 might play a role in the dephosphorylation of host nutrients to facilitate transport into the parasite. While this seems less likely if PfGAP50 is located in the ER/IMC compartments, alternative roles for the protein in early-stage parasites cannot be discounted. It is of interest to consider whether the phosphatase activity of PfGAP50 might play a role in the assembly of the glideosome complex. For example, phosphorylation of GAP45 has been shown to control the assembly of the *T. gondii* motor complex (21). It is important to note, however, that the phosphatase domain of PfGAP50 is predicted to face the lumen of the ER/IMC, while PfGAP45 is located in the parasite cytoplasm. Indeed, our finding that the truncated $PfGAP50_{1\text{-}369}$-GFP is released as a soluble protein into the PV supports the predicted orientation with the phosphatase domain facing the ER lumen. It remains possible, nonetheless, that PfGAP50 dephosphorylates structural components within the IMC lumen.

In this work, we found that when the acid phosphatase domain of PfGAP50 was replaced by GFP, the protein still appeared to be correctly trafficked; however, these parasites rapidly lost fluorescence, and the level of protein expression was very low (as assessed by Western analysis). This suggests that expression of PfGAP50 with a defective phosphatase domain (even in the presence of endogenous PfGAP50) may be deleterious to parasite growth. Attempts to generate transfectants in which *PfGAP50ΔAP-GFP* replaced the endogenous gene were not successful (unpublished data), again suggesting that the acid phosphatase domain may perform some important enzymatic activity or structural role. A similar growth disadvantage was observed in *T. gondii* when the phosphatase domain was replaced with the human purple phosphatase domain (20).

In conclusion, our data indicate that PfGAP50 plays an important role in the initial stages of the formation of the IMC of *P. falciparum*. We speculate that recruitment of a PfGAP50-containing cisternal compartment from the ER represents an early event in IMC formation. Further development of the IMC likely involves the expression and assembly of additional glideosome complex proteins, and we confirmed that PfGAP50

is attached to PfGAP45 and MTIP, thereby linking the IMC to the glideosome complex. Interactions with a subpellicular radial network of microtubules may facilitate extension of the IMC underneath the parasite plasma membrane. Our data show that the C-terminal membrane anchor of PfGAP50 is critical for correct trafficking and suggest that the phosphatase homology domain may also have an important function. Additional work may reveal a means of inhibiting PfGAP50 function, which would arrest merozoite development and stop parasite invasion.

ACKNOWLEDGMENTS

We thank Shannon Kenny and Sam Deed for technical assistance. We thank Akinola Adisa, La Trobe University, for generating the anti-PfGAPDH antiserum; Tony Holder, National Institute for Medical Research, London, United Kingdom, for donating anti-MTIP antibodies; and Brian Cooke, Monash University, Australia, for the anti-RhopH3 antiserum.

We acknowledge support from the Australian Research Council and the Australian National Health and Medical Research Council. C.B.W. is an Australian National Health and Medical Research Council Senior Research Fellow. M.W.A.D. is an Australian National Health and Medical Research Council Training Fellow. A.G.M. is an ARC Australian Research Fellow.

REFERENCES

1. **Abu Bakar, N. A., N. Klonis, E. Hanssen, C. Chan, and L. Tilley.** 2010. Digestive-vacuole genesis and endocytic processes in the early intraerythrocytic stages of *Plasmodium falciparum*. J. Cell Sci. **123:**441–450.
2. **Adisa, A., et al.** 2007. Re-assessing the locations of components of the classical vesicle-mediated trafficking machinery in transfected *Plasmodium falciparum*. Int. J. Parasitol. **37:**1127–1141.
3. **Adisa, A., et al.** 2003. The signal sequence of exported protein-1 directs the green fluorescent protein to the parasitophorous vacuole of transfected malaria parasites. J. Biol. Chem. **278:**6532–6542.
4. **Bannister, L. H., and A. R. Dluzewski.** 1990. The ultrastructure of red cell invasion in malaria infections: a review. Blood Cells **16:**257–292.
5. **Bannister, L. H., J. M. Hopkins, R. E. Fowler, S. Krishna, and G. H. Mitchell.** 2000. Ultrastructure of rhoptry development in *Plasmodium falciparum* erythrocytic schizonts. Parasitology **121:**273–287.
6. **Bannister, L. H., and G. H. Mitchell.** 2009. The malaria merozoite, forty years on. Parasitology **136:**1435–1444.
7. **Baum, J., T. W. Gilberger, F. Frischknecht, and M. Meissner.** 2008. Host-cell invasion by malaria parasites: insights from *Plasmodium* and *Toxoplasma*. Trends Parasitol. **24:**557–563.
8. **Baum, J., A. T. Papenfuss, B. Baum, T. P. Speed, and A. F. Cowman.** 2006. Regulation of apicomplexan actin-based motility. Nat. Rev. Microbiol. **4:**621–628.
9. **Baum, J., et al.** 2006. A conserved molecular motor drives cell invasion and gliding motility across malaria life cycle stages and other apicomplexan parasites. J. Biol. Chem. **281:**5197–5208.
10. **Bergman, L. W., et al.** 2003. Myosin A tail domain interacting protein (MTIP) localizes to the inner membrane complex of *Plasmodium* sporozoites. J. Cell Sci. **116:**39–49.
11. **Bozdech, Z., et al.** 2003. Expression profiling of the schizont and trophozoite stages of *Plasmodium falciparum* with a long-oligonucleotide microarray. Genome Biol. **4:**R9.
12. **Bullen, H. E., et al.** 2009. A novel family of Apicomplexan glideosome-associated proteins with an inner membrane-anchoring role. J. Biol. Chem. **284:**25353–25363.
13. **Deitsch, K., C. Driskill, and T. Wellems.** 2001. Transformation of malaria parasites by the spontaneous uptake and expression of DNA from human erythrocytes. Nucleic Acids Res. **29:**850–853.
14. **del Pilar Crespo, M., et al.** 2008. Artemisinin and a series of novel endoperoxide antimalarials exert early effects on digestive vacuole morphology. Antimicrob. Agents Chemother. **52:**98–109.
15. **de Melo, E. J., and W. de Souza.** 1997. A cytochemistry study of the inner membrane complex of the pellicle of tachyzoites of *Toxoplasma gondii*. Parasitol. Res. **83:**252–256.
16. **Dluzewski, A. R., et al.** 1992. Origins of the parasitophorous vacuole membrane of the malaria parasite, Plasmodium falciparum, in human red blood cells. J. Cell Sci. **102:**527–532.
17. **Duraisingh, M. T., A. G. Maier, T. Triglia, and A. F. Cowman.** 2003. Erythrocyte-binding antigen 175 mediates invasion in *Plasmodium falciparum* utilizing sialic acid-dependent and -independent pathways. Proc. Natl. Acad. Sci. U. S. A. **100:**4796–4801.
18. **Fidock, D. A., and T. E. Wellems.** 1997. Transformation with human dihydrofolate reductase renders malaria parasites insensitive to WR99210 but does not affect the intrinsic activity of proguanil. Proc. Natl. Acad. Sci. U. S. A. **94:**10931–10936.
19. **Frankland, S., et al.** 2006. Delivery of the malaria virulence protein PfEMP1 to the erythrocyte surface requires cholesterol-rich domains. Eukaryot. Cell **5:**849–860.
20. **Gaskins, E., et al.** 2004. Identification of the membrane receptor of a class XIV myosin in *Toxoplasma gondii*. J. Cell Biol. **165:**383–393.
21. **Gilk, S. D., E. Gaskins, G. E. Ward, and C. J. Beckers.** 2009. GAP45 phosphorylation controls assembly of the *Toxoplasma myosin* XIV complex. Eukaryot. Cell **8:**190–196.
22. **Green, J. L., et al.** 2006. The MTIP-myosin A complex in blood stage malaria parasites. J. Mol. Biol. **355:**933–941.
23. **Hanssen, E., et al.** 2010. Whole cell imaging reveals novel modular features of the exomembrane system of the malaria parasite, *Plasmodium falciparum*. Int. J. Parasitol. **40:**123–134.
24. **Hu, G., et al.** 2010. Transcriptional profiling of growth perturbations of the human malaria parasite *Plasmodium falciparum*. Nat. Biotechnol. **28:**91–98.
25. **Hu, K., et al.** 2002. Daughter cell assembly in the protozoan parasite *Toxoplasma gondii*. Mol. Biol. Cell **13:**593–606.
26. **Jones, M. L., E. L. Kitson, and J. C. Rayner.** 2006. *Plasmodium falciparum* erythrocyte invasion: a conserved myosin associated complex. Mol. Biochem. Parasitol. **147:**74–84.
27. **Keeley, A., and D. Soldati.** 2004. The glideosome: a molecular machine powering motility and host-cell invasion by Apicomplexa. Trends Cell Biol. **14:**528–532.
28. **Klonis, N., et al.** 2002. Fluorescence photobleaching analysis for the study of cellular dynamics. Eur. Biophys. J. **31:**36–51.
29. **Le Roch, K. G., et al.** 2003. Discovery of gene function by expression profiling of the malaria parasite life cycle. Science **301:**1503–1508.
30. **Lingelbach, K., and K. A. Joiner.** 1998. The parasitophorous vacuole membrane surrounding Plasmodium and Toxoplasma: an unusual compartment in infected cells. J. Cell Sci. **111:**1467–1475.
31. **Maier, A. G., et al.** 2003. *Plasmodium falciparum* erythrocyte invasion through glycophorin C and selection for Gerbich negativity in human populations. Nat. Med. **9:**87–92.
32. **Müller, I. B., et al.** 2010. Secretion of an acid phosphatase provides a possible mechanism to acquire host nutrients by *Plasmodium falciparum*. Cell Microbiol. **12:**677–691.
33. **Pinder, J. C., et al.** 1998. Actomyosin motor in the merozoite of the malaria parasite, Plasmodium falciparum: implications for red cell invasion. J. Cell Sci. **111:**1831–1839.
34. **Ranford-Cartwright, L. C., A. Sinha, G. S. Humphreys, and J. M. Mwangi.** 2010. New synchronization method for *Plasmodium falciparum*. Malar. J. **9:**170.
35. **Rees-Channer, R. R., et al.** 2006. Dual acylation of the 45 kDa gliding-associated protein (GAP45) in *Plasmodium falciparum* merozoites. Mol. Biochem. Parasitol. **149:**113–116.
36. **Satchell, J. F., et al.** 2005. Structure of glyceraldehyde-3-phosphate dehydrogenase from *Plasmodium falciparum*. Acta Crystallogr. D Biol. Crystallogr. **61:**1213–1221.
37. **Schermelleh, L., et al.** 2008. Subdiffraction multicolor imaging of the nuclear periphery with 3D structured illumination microscopy. Science **320:**1332–1336.
38. **Sim, B. K., C. E. Chitnis, K. Wasniowska, T. J. Hadley, and L. H. Miller.** 1994. Receptor and ligand domains for invasion of erythrocytes by *Plasmodium falciparum*. Science **264:**1941–1944.
39. **Soldati, D., and M. Meissner.** 2004. *Toxoplasma* as a novel system for motility. Curr. Opin. Cell Biol. **16:**32–40.
40. **Spielmann, T., et al.** 2006. A cluster of ring stage-specific genes linked to a locus implicated in cytoadherence in *Plasmodium falciparum* codes for PEXEL-negative and PEXEL-positive proteins exported into the host cell. Mol. Biol. Cell **17:**3613–3624.
41. **Topolska, A. E., A. Lidgett, D. Truman, H. Fujioka, and R. L. Coppel.** 2004. Characterization of a membrane-associated rhoptry protein of *Plasmodium falciparum*. J. Biol. Chem. **279:**4648–4656.
42. **WHO.** 2010. World Malaria Report 2010. WHO, Geneva, Switzerland. http://www.who.int/malaria/world_malaria_report_2010/world_malaria_report_2010.pdf.